Alzheimer Disease and Mild Cognitive Impairment: Integrated Pulsed Arterial Spin-labeling MRI and ^{18}F-FDG PET

*Isabelle Riederer, MD** • *Karl Peter Bohn, MD[1]** • *Christine Preibisch, PhD* • *Eva Wiedemann, MD* • *Claus Zimmer, MD* • *Panagiotis Alexopoulos, MD[2]* • *Stefan Förster, MD*

From the Department of Diagnostic and Interventional Neuroradiology (I.R., C.P., C.Z.), Department of Diagnostic and Interventional Radiology (I.R.), Department of Nuclear Medicine (K.P.B., E.W., S.F.), TUM Neuroimaging Center (TUM-NIC) (C.P., S.F.), and Departments of Psychiatry and Psychotherapy (P.A.), Klinikum Rechts der Isar, Technische Universität München, Ismaninger Str 22, 81675 Munich, Germany. Received March 13, 2017; revision requested April 27; revision received February 10, 2018; accepted March 5. **Address correspondence to** I.R. (e-mail: *Isabelle.riederer@tum.de*).

*I.R. and K.P.B. contributed equally to this work.

Current addresses:
[1]Department of Nuclear Medicine, Ulm University, Ulm, Germany.
[2]Department of Psychiatry, University Hospital of Rion, University of Patras, Greece.

Conflicts of interest are listed at the end of this article.

See also the editorial by Chiang in this issue.

Radiology 2018; 288:198–206 • https://doi.org/10.1148/radiol.2018170575 • Content code: NR

Purpose: To compare PET/MR hypoperfusion and hypometabolism in patients with Alzheimer disease (AD) and mild cognitive impairment (MCI) compared with healthy control (HC) participants.

Materials and Methods: Maps of cerebral blood flow (CBF; pulsed arterial spin-labeling [ASL] MRI), glucose metabolism (fluorine 18 [^{18}F] fluorodeoxyglucose [FDG] PET), and gray matter (GM) volume (structural T1-weighted MRI) were calculated from integrated PET/MR data in 45 patients with AD (mean age, 69 years ± 9 [standard deviation]; age range, 51–89 years), 20 patients with MCI (mean age, 64 years ± 10; age range, 45–82 years), and 11 HC participants (mean age, 65 years ± 8; age range, 54–80 years) between 2011 and 2014. After preprocessing, voxel-wise analyses of variance, volume of interest, and independent component analyses were performed for comparisons of CBF and glucose metabolism.

Results: Analyses revealed high overlap between components, regional and quantitative hypoperfusion, and hypometabolism in patients with AD compared with HC participants in precuneus, parietal, temporal, and occipital cortex. In patients with MCI compared with HC participants, FDG PET exclusively demonstrated quantitative hypometabolism and a component in the precuneus. Volume-of-interest analysis in global GM in patients with AD compared with HC participants showed lower CBF (42 mL/100 g per minute ± 8 vs 49 mL/100 g per minute ± 7, respectively; $P = .035$) and lower FDG uptake (0.8 ± 0.1 vs 1 ± 0.1, respectively; $P < .001$).

Conclusion: In patients with AD, pulsed ASL MRI revealed regional and quantitative abnormalities and components similar to ^{18}F-FDG PET with a reduced extent. In patients with MCI, ^{18}F-FDG PET exclusively demonstrated quantitative hypometabolism and a component in the precuneus, indicating higher sensitivity to detect preclinical AD compared with the currently used pulsed ASL MRI sequence.

Online supplemental material is available for this article.

Alzheimer disease (AD) is the most common cause of dementia and mild cognitive impairment (MCI). MCI is commonly referred to as a transitional state between cognition in normal aging and early dementia (1), and it often represents a prodromal phase of AD.

Even though there are only moderately effective therapeutic or preventive options currently available, a reliable decision-making diagnostic is particularly important in early disease stages. Other than neuropsychologic tests including the Mini-Mental State Examination, the guidelines from the National Institute on Aging–Alzheimer's Association suggest a variety of supportive diagnostic tools such as analysis of cerebrospinal fluid biomarkers and MRI and PET in the diagnostic work-up of patients with MCI (2) or AD (3). Although not widely available, fluorine 18 (^{18}F) fluorodeoxyglucose (FDG) PET is the most thoroughly established neuroimaging tool in the diagnosis of neurodegenerative dementia (4–6); it is on the basis of the measurement of hypometabolism, reflecting neuronal dysfunction. AD-typical FDG-hypometabolic alterations occur in the posterior parietotemporal association cortex, precuneus, and posterior cingulate cortex, (7) and usually precede cortical atrophy and clinical cognitive symptoms (8).

Arterial spin labeling (ASL) has been demonstrated to reveal typical brain perfusion abnormalities in patients with AD in the parietal cortex, the angular gyrus, the middle temporal cortex, and the precuneus (9). By using this technique, inflowing arterial blood water is magnetically labeled proximal to the region of interest using a 180° radiofrequency inversion pulse. Quantitative perfusion images are calculated from the subtraction of brain images without and with labeling of blood (10).

Abbreviations

AD = Alzheimer disease, ANOVA = analysis of variance, ASL = arterial spin labeling, CBF = cerebral blood flow, FDG = fluorodeoxyglucose, GM = gray matter, HC = healthy control, ICA = independent component analysis, MCI = mild cognitive impairment

Summary

Integrated fluordeoxyglucose and pulsed arterial spin-labeling PET/MR with voxel-based, voxel-of-interest–based, and independent component analysis demonstrates overlapping regional and quantitative measures of brain hypoperfusion and hypometabolism in patients with Alzheimer disease.

Implications for Patient Care

- Integrated PET/functional MRI in patients with Alzheimer disease and mild cognitive impairment makes it possible to reliably obtain different regional and quantitative measures of brain perfusion and brain metabolism.
- Volumetric T1-weighted structural brain data deliver complementary voxel-based morphometric information and can be used for partial volume correction of functional data.
- There is a high concordance between regional and quantitative measures of hypoperfusion and hypometabolism in patients with Alzheimer disease; therefore, pulsed arterial spin-labeling MRI may potentially become an alternative imaging modality to fluorine 18 fluorodeoxyglucose PET in the diagnosis of neurodegenerative Alzheimer disease.

The major advantages of ASL MRI compared with FDG PET are its noninvasiveness without injection of contrast agent and its lack of exposure to ionizing radiation.

Several studies (11–13) reported correlations between hypoperfusion in ASL and hypometabolism in FDG-PET in patients with AD; however, they were all performed on separate MR imagers and PET scanners with measurements at different time points.

We therefore aimed to compare different regional and quantitative measures of integrated PET/MRI hypoperfusion and hypometabolism in patients with AD and MCI compared with healthy control (HC) participants.

Materials and Methods

Study Sample

Our study protocol was approved by the local ethics committee (medical faculty of the Technical University of Munich) and conducted in accordance with the 1964 Declaration of Helsinki. Written informed consent to undergo imaging was obtained from all participants. Imaging in patients was part of the clinical routine work up because of cognitive decline, whereas imaging in HC participants was approved by the German Radiation Protection Agency.

Participants were examined at the Center for Cognitive Disorders of the Departments of Psychiatry and Psychotherapy and the Department of Nuclear Medicine of the Technical University of Munich between 2011 and 2014. Our participants were composed of the following: 45 consecutive patients with AD (mean age, 69 years ± 9 [standard deviation]; age range, 51–89 years), which consisted of 25 women (mean age, 67 years ± 10; age range, 51–89 years) and 20 men (mean age, 72 years ± 8; age range, 58–84 years); 20 patients with MCI (mean age, 64 years ± 10; age range, 45–82 years), which consisted of 10 women (mean age, 72 years ± 5; age range, 62–79 years) and 10 men (mean age, 67 years ± 11; age range, 45–82 years); and 11 HC participants (mean age, 65 years ± 8; age range, 54–80 years), which consisted of six women (mean age, 63 years ± 7; age range, 54–71 years) and five men (mean age, 67 years ± 8; age range, 58–80 years). There were no statistically significant differences in age between men and women by using two-sided *t* tests (difference in age between all men and women, $P = .33$; between women and men with AD, $P = .10$; between women and men with MCI, $P = .24$; and between HC women and men, $P = .43$). Table 1 summarizes sex distribution, mean age, age range, average Mini-Mental State Examination score, and mean education time. A subgroup of patients were previously analyzed in an earlier study (14) in which we proposed an adapted voxel-based probabilistic comparison method to quantify abnormalities in individual AD patients only on the basis of pulsed ASL images. There is no overlap regarding the methods or results presented in our current study.

Patients with AD fulfilled the criteria of the International Classification of Diseases–10th edition system for dementia and the criteria of the National Institute of Neurologic and Communicative Disorders and Stroke–Alzheimer's Disease and Related Disorders Association for probable AD (15). All patients with AD were treated with cholinesterase inhibitors and/or memantine without changes in the dose of medication for at least 3 months before undergoing PET/MRI. The diagnosis of MCI followed the revised consensus criteria of the International Working Group on MCI (16). HC participants were recruited prospectively by means of advertisement, were free of cognitive disorders according to neuropsychologic testing and Mini-Mental State Examination above 27, and had no substantial illness or medical treatments that could have affected neuronal activity or cerebral blood flow (CBF). Exclusion criteria were current or previous psychiatric or neurologic disorders (eg, major depression, posttraumatic stress disorders, stroke, seizure disorders, head injury, and schizophrenia) and contraindications to MRI such as metal implants, cardiac pace makers, claustrophobia, or pregnancy. Five patients were excluded because of severe motion artifacts and were not included in the reported numbers. None of the HC participants were excluded. Figure 1 shows the flowchart of the initial participant population.

All details about PET/MR image acquisition and data analysis are provided in the Appendix E1 (online).

Results

Pulsed ASL and Reduced CBF

Voxel-wise analysis of varidance (ANOVA) demonstrated a pattern of reduced CBF in bilateral parietotemporal cortex, precuneus, and posterior cingulate cortex in patients with AD compared with HC participants.

In patients with AD compared with patients with MCI, voxel-wise ANOVA demonstrated a pattern of reduced CBF in bilateral parietal cortex, precuneus, left inferior temporal cortex, and left temporal mesial cortex. Voxel-wise ANOVA revealed

no CBF reductions between patients with MCI and HC participants. Spatial maps of the CBF voxel-wise ANOVA that show the respective regional patterns of reduced CBF are presented in Figure 2 (blue color).

Results from quantitative volume-of-interest–based analyses in a global gray matter (GM) volume of interest and in different anatomic GM volumes of interest are listed in Table 2.

The independent component analysis (ICA) led to one significant component for each of the examinations of all three groups together, AD and HC participants, and AD and MCI. These components involved a small area of the parietal lobe around the angular gyrus and the precuneus (Fig 3) and partly posterior cingulate on both sides. No significant components were found at the analyses of MCI and HC participants. All components (including the nonsignificant ones) are on Figure E1 (online). Additional information on the significant components can be found in Table E1 (online).

Table 1: Demographic Data of Our Examined Study Sample

Parameter	AD	MCI	HC
Total no. of participants	45	20	11
Women*	25 (55.6)	10 (50.0)	6 (54.5)
Mean age (y)	69 ± 9 (51–89)	64 ± 10 (45–82)	65 ± 8 (54–80)
Women	67 ± 10 (51–89)	72 ± 5 (62–79)	63 ± 7 (54–71)
Men	72 ± 8 (58–84)	67 ± 11 (45–82)	67 ± 8 (58–80)
MMSE score	22.0 ± 4.0	26.5 ± 2.1	28.5 ± 1.1
Education (y)	12.6 ± 3.8	12.3 ± 3.3	12.4 ± 3.0

Note.—Unless otherwise indicated, data are mean ± standard deviation and data in parentheses are range. Difference in age between patients with Alzheimer disease and those with mild cognitive impairment: $P = .87$; Alzheimer disease and healthy control participants: $P = .16$; mild cognitive impairment and healthy control participants, $P = .14$. Difference in age between women and men with Alzheimer disease, $P = .10$; with MCI, $P = .24$; and in healthy control participants, $P = .43$. AD = Alzheimer disease, HC = healthy control participants, MCI = mild cognitive impairment, MMSE = Mini-Mental State Examination.

* Data in parentheses are percentage.

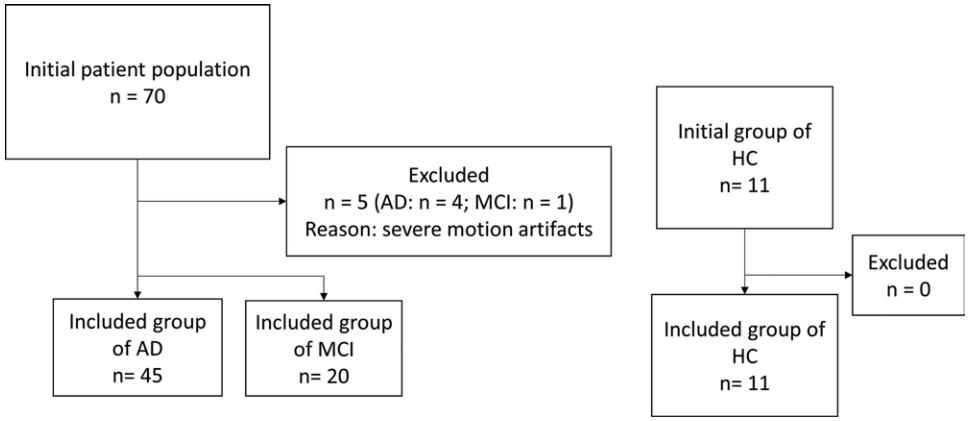

Figure 1: Flowchart shows the initial participant population and those excluded because of severe motion artifacts. AD = Alzheimer disease, HC = healthy control participants, MCI = mild cognitive impairment.

^{18}F-FDG PET and Reduced FDG Uptake

Voxel-wise ANOVA revealed a pattern of reduced FDG uptake in the bilateral parietotemporal cortex, precuneus, posterior cingulate cortex, mesial temporal cortex, and mesial- and dorsolateral prefrontal cortex in patients with patients with AD compared with HC participants.

In patients with AD compared with patients with MCI, voxel-wise ANOVA showed a pattern of reduced FDG uptake in the bilateral parietotemporal cortex, precuneus, posterior cingulate cortex, and mesial prefrontal cortex. In patients with MCI compared with HC, voxel-wise ANOVA demonstrated a pattern of reduced FDG uptake in the bilateral inferior parietal cortex, superior temporal cortex, precuneus, posterior cingulate cortex, mesial temporal cortex, and right dorsolateral prefrontal cortex.

Spatial maps of the ^{18}F-FDG PET voxel-wise ANOVA showing the respective regional patterns of reduced FDG uptake are in Figure 2. Results from quantitative volume of interest–based analysis in a global GM volume of interest and in different anatomic GM volumes of interest are listed in Table 3.

ICA analysis led to at least one statistically significant component, and the analysis of AD and HC was only one that led to three significant components. The significant components each involved the precuneus (Fig 3) and posterior cingulate. Furthermore, parts of the superior parietal lobe were included in the significant components for the analyses of AD, MCI and HC, and AD and MCI. The analysis for AD and HC showed a further extension of the significant components throughout the parietal and temporal lobes on both sides. The component for MCI and HC stayed limited to the precuneus, posterior cingulate, and orbitofrontal cortex. All components (including the nonsignificant ones) are in Figure E2 (online). Additional information on the significant components can be found in Table E2 (online).

Voxel-based Morphometry and GM Volume Decrease

In patients with AD compared with HC participants, voxel-wise ANOVA revealed a pattern of decreased GM volume in bilateral parietotemporal cortex, precuneus, posterior cingulate cortex, mesial temporal cortex, and left mesial prefrontal cortex.

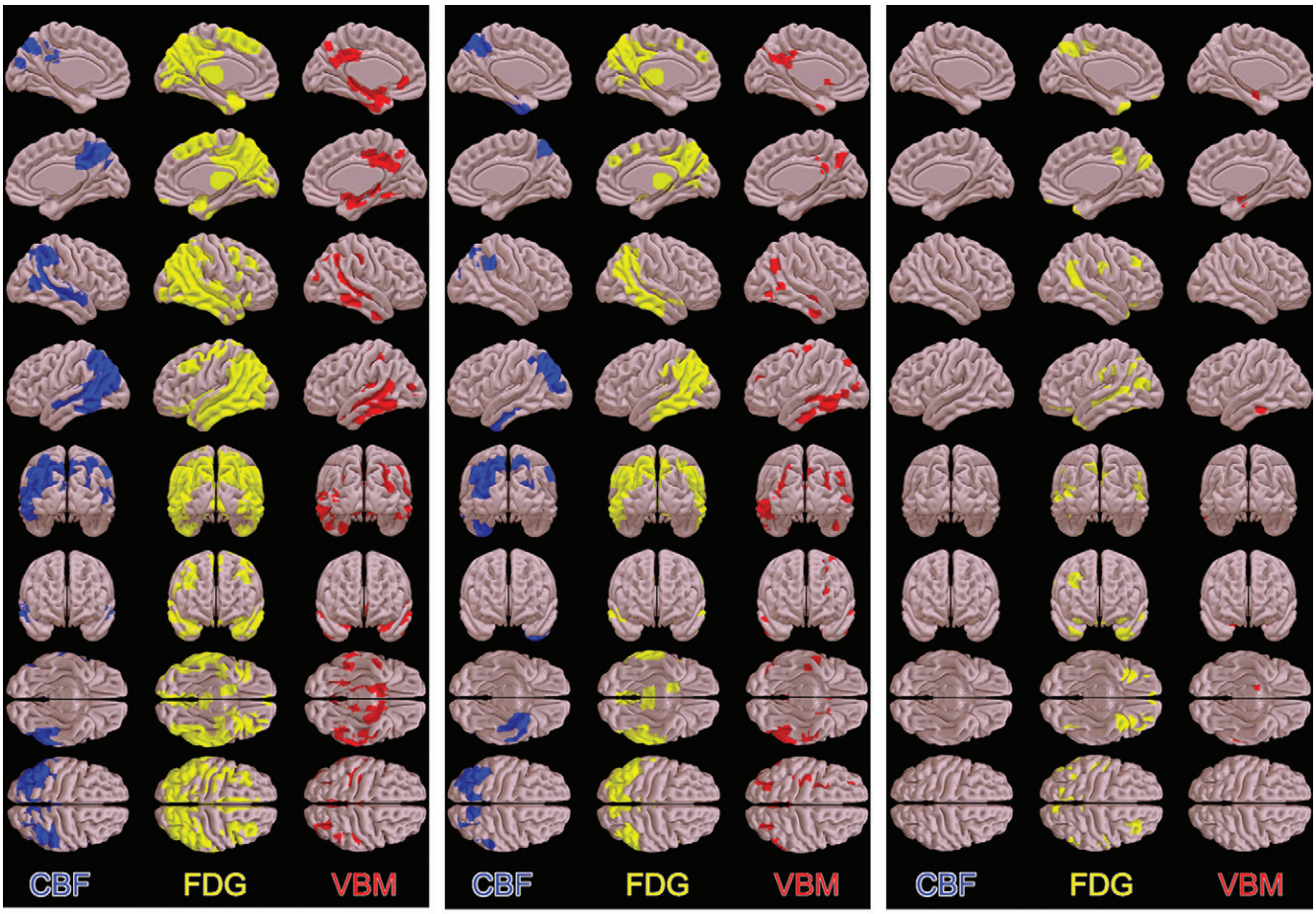

Figure 2: Spatial maps of the results of the voxel-wise analysis of variance with the patterns of reduced cerebral blood flow (CBF; pulsed arterial spin-labeling MRI, blue), reduced fluorodeoxyglucose (FDG) uptake (^{18}F-FDG PET, yellow), and decreased gray-matter volume (voxel-based morphometry [VBM], red) in **(a)** patients with Alzheimer disease compared with healthy control participants, **(b)** patients with AD compared with patients with mild cognitive impairment, and **(c)** patients with mild cognitive impairment compared with healthy control participants ($P < .001$, uncorrected).

In patients with AD compared with patients with MCI, voxel-wise ANOVA demonstrated a pattern of decreased GM volume in bilateral inferior temporal cortex, precuneus, posterior cingulate cortex, right inferior parietal cortex, left mesial temporal cortex, and left dorsolateral prefrontal cortex. In patients with MCI compared with HC participants, voxel-wise ANOVA showed a pattern of decreased GM volume in the right mesial temporal cortex and left inferior temporal cortex. Spatial maps of the voxel-based morphometry voxel-wise ANOVA that show the respective regional patterns of decreased GM volume are in Figure 2.

Figure 4 shows overlays of the voxel-wise ANOVA patterns of reduced CBF (pulsed ASL), reduced FDG uptake (^{18}F-FDG PET) and decreased GM volume (voxel-based morphometry), enabling a direct regional comparison of all three modalities in patients with AD compared with HC participants (Fig 4, *A*) and in patients with AD compared with patients with MCI (Fig 4, *B*).

Overall, the largest number of significant components could be found for the ICA of the voxel-based morphometry data for all analyses except the one for MCI and HC, which did not lead to statistically significant components. These significant components showed their main extension throughout the parietal and temporal lobes on both sides. The deep gray matter was also included in some components. Further details on all significant components are listed in Table E3 (online). All components (including the nonsignificant ones) can be found on Figure E3 (online).

Discussion

Integrated ^{18}F-FDG and pulsed ASL PET/MR that used voxel-based, volume-of-interest–based, and independent component analyses demonstrated highly overlapping regional and quantitative measures of brain hypoperfusion and hypometabolism in patients with AD.

Previous studies (9,17) of ASL MRI reported regional hypoperfusion in patients with AD in the parietal cortex, precuneus, temporal cortex, and posterior cingulate cortex, whereas previous studies (7,8,18,19) of FDG PET reported hypometabolism in the same brain regions in patients with AD, all representing regions typically affected by neurodegenerative AD and all brain regions we detected in this study.

Our results for ^{18}F-FDG PET in patients with MCI revealed the most extended abnormality pattern and an exclusively

Table 2: Results of the Volume-of-Interest Analysis of CBF (Pulsed ASL MRI)

Parameter	CBF Corrected for Partial-Volume Effects (mL/100 g per min)			One-way ANOVA*	Tukey Post Hoc Analysis*		
	HC	MCI	AD		HC > AD	MCI > AD	HC > MCI
Global GM (all VOIs)	48.8 ± 6.8	45.9 ± 9.6	41.7 ± 7.9	.222	.035	.158	.615
Frontal lobe							
Inferior frontal, operculum	39.8 ± 8.5	39.2 ± 12.5	42.9 ± 11.5	.421	.701	.448	.988
Inferior frontal, orbital	47.3 ± 8.8	46.6 ± 12.1	44.2 ± 12.7	.639	.734	.735	.990
Inferior frontal, tri.	31.8 ± 8.4	38.9 ± 17.5	43.1 ± 13.5	.057	.051	.514	.377
Rolandic operculum	66.8 ± 14.0	65.5 ± 11.5	65.1 ± 11.2	.913	.904	.992	.953
Insula	51.9 ± 10.6	53.3 ± 9.3	51.9 ± 9.1	.845	>.999	.840	.915
Paracentral lobule	47.3 ± 22.1	39.0 ± 19.4	41.1 ± 2.9	.558	.639	.932	.538
Cingulum							
Middle cingulum	48.3 ± 11.0	44.5 ± 15.3	44.3 ± 13.3	.679	.666	.999	.735
Posterior cingulum	37.8 ± 8.5	33.9 ± 13.6	29.3 ± 13.9	.119	.144	.397	.719
Deep GM							
Caudate	31.6 ± 7.1	28.8 ± 13.2	28.7 ± 11.5	.745	.733	.999	.793
Putamen	45.7 ± 12.7	46.8 ± 11.6	46.9 ± 9.7	.945	.942	>.999	.957
Pallidum	23.0 ± 6.1	27.2 ± 8.9	26.5 ± 8.2	.356	.406	.944	.354
Thalamus	49.5 ± 10.3	51.9 ± 17.5	47.6 ± 16.3	.597	.930	.572	.916
Temporal lobe							
Heschl	87.7 ± 15.1	79.3 ± 11.3	76.5 ± 13.7	.049	.038	.713	.220
Superior temporal	73.7 ± 12.2	67.5 ± 11.4	61.5 ± 1.1	.003	.004	.105	.285
Superior temporal pole	54.0 ± 13.0	51.1 ± 12.5	45.0 ± 9.8	.020	.044	.107	.753
Middle temporal	53.3 ± 7.5	47.4 ± 12.5	39.2 ± 11.0	<.001	.001	.019	.339
Middle temporal pole	59.6 ± 12.8	51.0 ± 17.1	49.0 ± 17.4	.179	.153	.899	.364
Inferior temporal	30.2 ± 9.1	25.9 ± 13.9	19.4 ± 9.9	.006	.012	.075	.548
Fusiform gyrus	53.8 ± 7.8	47.0 ± 14.0	46.9 ± 14.8	.319	.303	.999	.399
Limbic system							
Hippocampus	57.6 ± 11.2	59.3 ± 8.4	57.2 ± 9.0	.681	.990	.658	.870
Parahippocampus	64.8 ± 11.1	62.3 ± 8.9	63.2 ± 9.4	.775	.875	.923	.755
Amygdala	53.3 ± 11.5	52.5 ± 12.5	56.6 ± 14.5	.351	.318	.906	.577
Parietal lobe							
Postcentral	41.0 ± 7.9	36.6 ± 12.8	4.6 ± 11.5	.394	.995	.398	.566
Superior parietal	24.6 ± 11.4	21.3 ± 15.7	13.1 ± 8.8	.002	.009	.023	.718
Inferior parietal	45.1 ± 7.9	37.1 ± 16.3	27.7 ± 11.6	<.001	<.001	.019	.213
Supramarginal	47.6 ± 7.9	44.2 ± 11.0	41.1 ± 1.8	.158	.167	.522	.669
Angular	42.8 ± 11.8	37.5 ± 17.9	27.5 ± 12.3	.001	.005	.025	.570
Precuneus	44.7 ± 11.0	41.1 ± 14.5	33.0 ± 14.3	.016	.040	.086	.774
Occipital lobe							
Calcarine	64.2 ± 7.7	58.5 ± 12.8	56.8 ± 17.3	.351	.318	.906	.577
Cuneus	57.6 ± 7.6	52.0 ± 15.9	43.8 ± 19.8	.037	.057	.199	.671
Superior occipital	34.1 ± 10.6	29.5 ± 15.1	22.1 ± 13.0	.013	.025	.103	.637
Middle occipital	29.5 ± 12.3	25.0 ± 15.6	14.5 ± 1.1	<.001	.001	.005	.589
Lingual gyrus	69.0 ± 11.5	63.1 ± 14.8	62.5 ± 13.3	.355	.329	.987	.471

Note.—Data are mean ± standard deviation unless otherwise noted. Cerebral blood flow was corrected for partial volume effects in a global gray matter volume of interest and in different anatomic gray matter volumes of interest for healthy control participants, patients with mild cognitive impairment and Alzheimer disease by using a one-way analysis of variance with Tukey post hoc analysis. *P* values less than .05 indicate statistical significance. AD = Alzheimer disease, ANOVA = analysis of variance, ASL = arterial spin labeling, CBF = cerebral blood flow, GM = gray matter, HC = healthy control participants, MCI = mild cognitive impairment, VOI = volume of interest.

* Data are *P* values; $P < .05$ indicates statistical significance.

quantitative significant result, and a significant component in the precuneus. This might indicate that ^{18}F-FDG PET has a higher sensitivity for detecting abnormalities in early preclinical stages of neurodegenerative AD compared with other modalities. According to the updated hypothetical biomarker model of AD (20), this would fit into a scenario where hypometabolism as a marker of early neuronal dysfunction might be observed before structural brain volume changes in this region are evident.

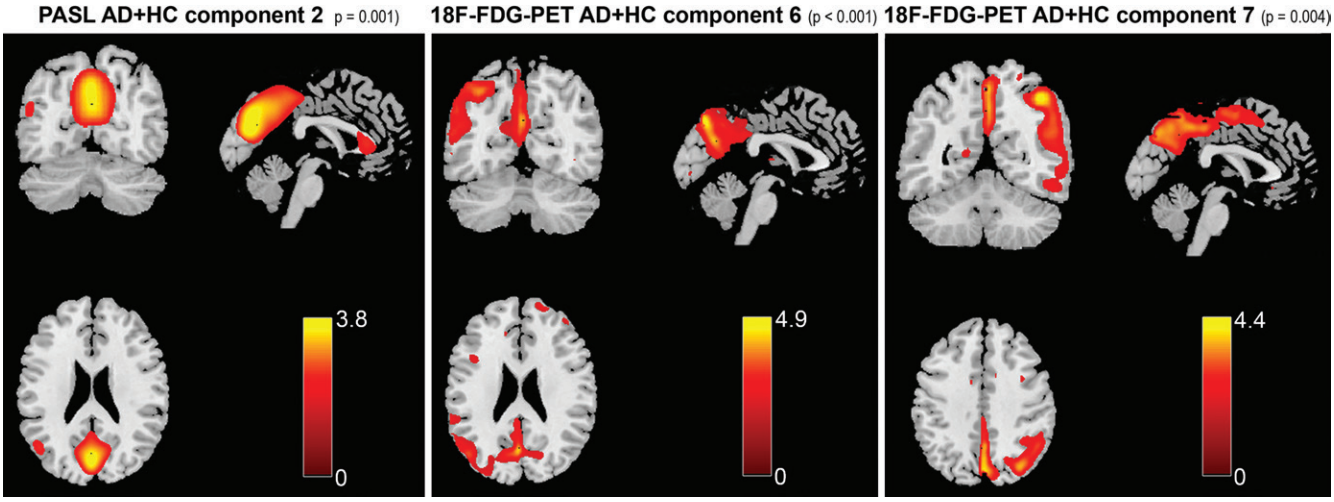

Figure 3: Exemplary views (threshold, $|Z|>2$) of significant components involving the precuneus and posterior cingulate for patients with Alzheimer disease (AD) and healthy control (HC) participants by using pulsed ASL (left) and fluorine 18 (^{18}F) fluorodeoxyglucose (FDG) PET (middle and right). The component number and *P* values resulting from the independent component analysis source-based morphometry statistical analyses are in Tables E1 and E2 (online).

However, cerebral metabolism and perfusion are both functional brain measurements and are functionally related to each other. The neurophysiologic basis for this functional relation is a tight regulatory link between neuroglial metabolic coupling, which is a central physiologic principle of brain function that provided the basis for FDG PET brain imaging (21) and perfusion in the brain (22–24). Therefore, one would expect that pulsed ASL MRI shows an abnormality pattern of hypoperfusion and significant volume-of-interest–based results and significant components similar to ^{18}F-FDG PET in our comparison of patients with MCI and HC participants because previous ASL MRI studies (9,25) demonstrated reduced CBF in patients with MCI in the parietotemporal cortex in the precuneus and posterior cingulate cortices.

A potential reason for the discrepancy of our results with previously reported significant CBF reductions in patients with MCI might be the limited signal-to-noise ratio of pulsed ASL MRI compared with ^{18}F-FDG PET and other different technical approaches in use for ASL MRI that are not directly comparable to our results. The original approach, continuous ASL (10), applies a long (~1–2 seconds) continuous inversion pulse on a thin labeling section (~1 cm) proximal to the imaging volume of interest. However, this technique is limited by hardware restrictions on clinical imagers and high-power deposition (ie, specific absorption rate), especially at higher field strength of 3.0 T and above. Therefore, clinical studies use pulsed ASL techniques (26), which apply a short inversion pulse (~4 msec) on a thick labeling section (~10 cm); thus, pulsed ASL techniques are used more frequently in our current study and in a previous study from our group (9). A further, more recent technical development is pseudocontinuous ASL, in which continuous labeling is achieved by a train of short labeling pulses leading to a high labeling efficiency with reduced power deposition as compared with continuous ASL. This technique was recently recommended by the perfusion study group of the International Society of Magnetic Resonance in Medicine as a standard (27) because of its superior signal-to-noise ratio, and it was already successfully used in previous neurodegenerative studies in patients with AD or frontotemporal dementia (13). However, on our integrated PET/MR scanner, pseudocontinuous ASL was not implemented; we therefore had to use a pulsed ASL sequence, which did not cover the whole brain volume.

Overall, the results of our statistical parametric mapping voxel-wise ANOVAs are consistent with the results of our ICA. Similar to voxel-wise ANOVAs, only ^{18}F-FDG PET led to significant results for the comparison of MCI patients and HC participants, supporting the mentioned theory of a potentially higher sensitivity of the PET method. The results of the ICA are consistent with previous studies that performed ICA on patients with AD and MCI for structural MRI data (28–32) and for ^{18}F-FDG PET data (28,30,32–34). We are not aware of any previous studies that analyzed pulsed ASL data in a setting similar to ours. So far, ICA studies that used source-based morphometry mainly analyzed structural MRI data in patients with schizophrenia (35,36) and, to a lesser degree, healthy participants (37,38) and patients with Huntington disease (39). Therefore, by applying ICA to three imaging modalities and especially by applying source-based morphometry to patients with AD and MCI for all three modalities, we offer an application of this method. In our current study, we explicitly decided not to perform joint ICA or parallel ICA (*http://mialab.mrn.org/software/fit*) to independently search for common intermodality components because we aimed to evaluate each modality on its own to compare the performance independently and achieve a better comparability to the setting of our statistical parametric mapping voxel-wise ANOVAs.

The additionally acquired volumetric T1-weighted structural brain data according to our voxel-based morphometry and ICA results delivered helpful and complementary information to pulsed ASL MRI and FDG PET. It exclusively revealed abnormal brain regions in patients with AD with reduced gray matter volume and associated components in the mesial- and inferior

Table 3: Results of the Volume-of-Interest Analysis of ^{18}F-FDG PET

Parameter	Normalized FDG Uptake			One-way ANOVA	Tukey Post Hoc Analysis		
	HC	MCI	AD		HC > AD	MCI > AD	HC > MCI
Global GM (all VOIs)	0.90 ± 0.06	0.84 ± 0.08	0.80 ± 0.07	<.001	<.001	.032	.116
Frontal lobe							
Inferior frontal, operculum	0.95 ± 0.11	0.89 ± 0.13	0.83 ± 0.12	.008	.012	.128	.435
Inferior frontal, orbital	1.06 ± 0.11	0.94 ± 0.13	0.93 ± 0.14	.015	.011	.947	.046
Inferior frontal, tri.	0.92 ± 0.10	0.86 ± 0.15	0.81 ± 0.14	.060	.057	.470	.427
Rolandic operculum	1.03 ± 0.12	1.00 ± 0.16	0.94 ± 0.14	.116	.187	.276	.882
Insula	1.06 ± 0.09	1.02 ± 0.13	0.96 ± 0.13	.023	.039	.158	.637
Paracentral lobule	0.88 ± 0.11	0.82 ± 0.14	0.80 ± 0.15	.255	.226	.856	.512
Cingulum							
Middle cingulum	1.12 ± 0.17	0.97 ± 0.16	0.94 ± 0.15	.003	.002	.742	.029
Posterior cingulum	0.88 ± 0.10	0.79 ± 0.15	0.72 ± 0.16	.021	.020	.356	.307
Deep GM							
Caudate	0.77 ± 0.20	0.75 ± 0.24	0.66 ± 0.17	.099	.189	.219	.925
Putamen	1.02 ± 0.11	1.02 ± 0.19	0.96 ± 0.17	.309	.554	.366	.999
Pallidum	0.45 ± 0.07	0.48 ± 0.13	0.42 ± 0.12	.120	.598	.112	.829
Thalamus	0.79 ± 0.09	0.81 ± 0.13	0.78 ± 0.12	.548	.908	.523	.913
Temporal lobe							
Heschl	1.22 ± 0.15	1.09 ± 0.15	1.02 ± 0.16	<.001	<.001	.186	.056
Superior temporal	1.10 ± 0.08	1.00 ± 0.14	0.93 ± 0.13	<.001	<.001	.144	.069
Superior temporal pole	0.78 ± 0.08	0.68 ± 0.12	0.63 ± 0.13	.001	.001	.234	.066
Middle temporal	1.03 ± 0.10	0.93 ± 0.12	0.82 ± 0.14	<.001	<.001	.009	.091
Middle temporal pole	0.80 ± 0.08	0.68 ± 0.11	0.69 ± 0.11	.007	.009	.901	.009
Inferior temporal	0.97 ± 0.08	0.89 ± 0.13	0.79 ± 0.13	<.001	<.001	.009	.303
Fusiform gyrus	1.01 ± 0.08	0.91 ± 0.17	0.89 ± 0.14	.030	.023	.783	.133
Limbic system							
Hippocampus	0.79 ± 0.10	0.75 ± 0.12	0.71 ± 0.10	.062	.069	.364	.554
Parahippocampus	0.92 ± 0.06	0.86 ± 0.11	0.83 ± 0.10	.026	.022	.467	.257
Amygdala	0.95 ± 0.06	0.89 ± 0.12	0.89 ± 0.10	.145	.126	.967	.256
Parietal lobe							
Postcentral	0.87 ± 0.10	0.81 ± 0.14	0.80 ± 0.13	.329	.297	.965	.480
Superior parietal	0.83 ± 0.14	0.77 ± 0.17	0.67 ± 0.16	.003	.007	.051	.520
Inferior parietal	0.98 ± 0.11	0.88 ± 0.17	0.75 ± 0.15	<.001	<.001	.007	.185
Supramarginal	0.93 ± 0.11	0.86 ± 0.13	0.79 ± 0.13	.003	.004	.112	.283
Angular	1.01 ± 0.11	0.87 ± 0.15	0.72 ± 0.16	<.001	<.001	.001	.041
Precuneus	1.26 ± 0.10	1.00 ± 0.15	0.98 ± 0.17	<.001	<.001	.013	.045
Occipital lobe							
Calcarine	1.31 ± 0.12	1.13 ± 0.16	1.11 ± 0.16	.002	.001	.955	.008
Cuneus	1.25 ± 0.14	1.10 ± 0.17	0.99 ± 0.18	<.001	<.001	.072	.047
Superior occipital	0.97 ± 0.11	0.88 ± 0.16	0.80 ± 0.16	.006	.006	.207	.237
Middle occipital	0.95 ± 0.12	0.89 ± 0.15	0.78 ± 0.16	.001	.002	.026	.451
Lingual gyrus	1.19 ± 0.10	1.08 ± 0.16	1.08 ± 0.14	.055	.050	.999	.095

Note.—Unless otherwise indicated, data are mean ± standard deviation. Data are normalized FDG uptake corrected for partial volume effects in a global gray matter volume of interest and in different anatomic gray matter volumes of interest for healthy control participants, patients with mild cognitive impairment, and patients with Alzheimer disease by using a one-way analysis of variance with Tukey post hoc analysis. AD = Alzheimer disease, ANOVA = analysis of variance, ASL = arterial spin labeling, CBF = cerebral blood flow, GM = gray matter, HC = healthy control participants, MCI = mild cognitive impairment, VOI = volume of interest.

* Data are *P* values. *P* values less than .05 indicate statistical significance.

temporal lobe, brain regions which were previously reported (40) in a meta-analysis to show structural alterations predictive of AD.

Our PET/MR study was designed to compare different regional and quantitative measures of hypoperfusion and hypometabolism. Future studies are necessary to examine the clinical benefit of such a comprehensive integrated functional and structural PET/MR protocol in the routine workup of patients with neurodegenerative AD on a single-subject level.

We speculate that improvements and further standardization in ASL MR image acquisition (27) and analysis, leading to increased signal-to-noise ratio and diagnostic sensitivity, may pave the way for individual single-subject evaluations to be an alternative to ^{18}F-FDG PET in the future diagnosis of neurodegenerative dementia. In a recent work (14) we introduced a computer-aided diagnostic tool that uses an adapted voxel-based morphometry technique and provides a CBF model of the healthy population.

Our current study has limitations. First, the sample size was small. Second, although major structural cerebrovascular changes were ruled out at T2-weighted fluid-attenuated inversion recovery MRI, we did not perform MR angiography to investigate blood vessels and we did not account for factors inducing arterial blood flow changes (ie, carotid artery stenoses) that could have had an effect on CBF measurements. Third, patient diagnoses were on the basis of clinical examination. Histopathologic confirmation or supportive measures (β amyloid, apolipoprotein ε4 allele status) were not available. Fourth, we used a pulsed ASL sequence, which did not cover the whole brain volume and hence did not allow us to compare abnormalities in the frontal lobes that were not included.

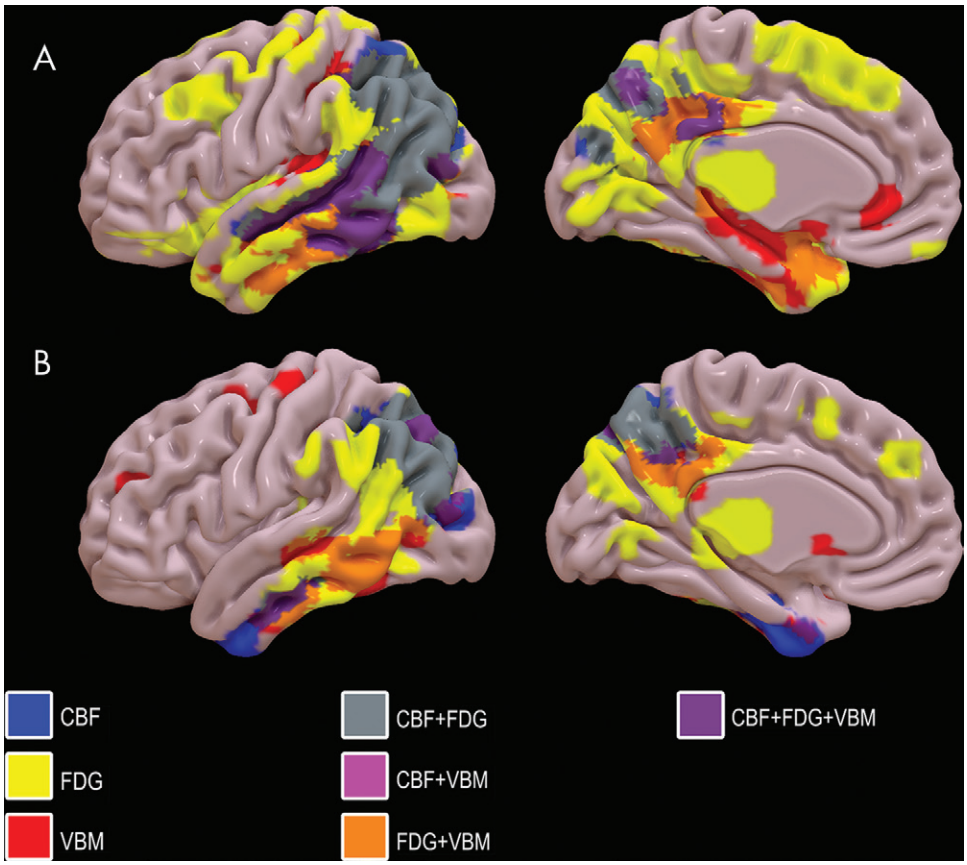

Figure 4: Overlays of patterns of reduced cerebral blood flow (CBF; pulsed arterial spin labeling, blue), reduced fluorodeoxyglucose (FDG) uptake (FDG PET, yellow), and decreased gray matter volume (voxel-based morphometry [VBM], red) in *A*, patients with Alzheimer disease compared with healthy control participants, and *B*, patients with Alzheimer disease compared with patients with mild cognitive impairment ($P < .001$ uncorrected by using Surf Ice [*https://www.nitrc.org/projects/surfice/*]). Gray, magenta, orange, and purple indicate the overlap of significant differences for different modalities. The field of view of the pulsed arterial spin labeling is limited to a part of the brain including the bilateral parietal, temporal and posterior cingulate cortices.

To conclude, our study suggests that within integrated PET/MRI data in patients with AD compared with HC participants, pulsed ASL MRI delivers comparable regional abnormality patterns, quantitative volume of interest–based measures, and significant components to ^{18}F-FDG PET. In patients with MCI, only ^{18}F-FDG PET revealed quantitatively reduced ^{18}F-FDG uptake and a corresponding significant component in the precuneus, a brain region that is typically involved in early neurodegenerative AD, whereas pulsed ASL MRI did not reveal significant results. The latter discrepancy in MCI might be attributable to technical limitations of the applied pulsed ASL sequence with an inferior signal-to-noise ratio.

Author contributions: Guarantors of integrity of entire study, I.R., K.P.B., S.F.; study concepts/study design or data acquisition or data analysis/interpretation, all authors; manuscript drafting or manuscript revision for important intellectual content, all authors; approval of final version of submitted manuscript, all authors; agrees to ensure any questions related to the work are appropriately resolved, all authors; literature research, I.R., K.P.B., C.P., E.W., C.Z., S.F.; clinical studies, I.R., K.P.B., E.W., C.Z., P.A., S.F.; experimental studies, C.Z.; statistical analysis, I.R., K.P.B., E.W., C.Z., S.F.; and manuscript editing, I.R., K.P.B., C.P., C.Z., P.A., S.F.

Disclosures of Conflicts of Interest: **I.R.** disclosed no relevant relationships. **K.P.B.** disclosed no relevant relationships. **C.P.** disclosed no relevant relationships. **E.W.** disclosed no relevant relationships. **C.Z.** Activities related to the present article: disclosed no relevant relationships. Activities not related to the present article: disclosed payment to author for lectures from Bayer. Other relationships: disclosed no relevant relationships. **P.A.** disclosed no relevant relationships. **S.F.** disclosed no relevant relationships.

References

1. Petersen RC, Negash S. Mild cognitive impairment: an overview. CNS Spectr 2008;13(1):45–53.
2. Albert MS, DeKosky ST, Dickson D, et al. The diagnosis of mild cognitive impairment due to Alzheimer's disease: recommendations from the National Institute on Aging-Alzheimer's Association workgroups on diagnostic guidelines for Alzheimer's disease. Alzheimers Dement 2011;7(3):270–279.
3. McKhann GM, Knopman DS, Chertkow H, et al. The diagnosis of dementia due to Alzheimer's disease: recommendations from the National Institute on Aging-Alzheimer's Association workgroups on diagnostic guidelines for Alzheimer's disease. Alzheimers Dement 2011;7(3):263–269.
4. de Leon MJ, Convit A, Wolf OT, et al. Prediction of cognitive decline in normal elderly subjects with 2-[(18)F]fluoro-2-deoxy-D-glucose/poitron-emission tomography (FDG/PET). Proc Natl Acad Sci U S A 2001;98(19):10966–10971.
5. Minoshima S, Frey KA, Koeppe RA, Foster NL, Kuhl DE. A diagnostic approach in Alzheimer's disease using three-dimensional stereotactic surface projections of fluorine-18-FDG PET. J Nucl Med 1995;36(7):1238–1248.
6. Silverman DH. Brain 18F-FDG PET in the diagnosis of neurodegenerative dementias: comparison with perfusion SPECT and with clinical evaluations lacking nuclear imaging. J Nucl Med 2004;45(4):594–607.
7. Förster S, Yousefi BH, Wester HJ, et al. Quantitative longitudinal interrelationships between brain metabolism and amyloid deposition during a 2-year fol-

low-up in patients with early Alzheimer's disease. Eur J Nucl Med Mol Imaging 2012;39(12):1927–1936.
8. Minoshima S, Giordani B, Berent S, Frey KA, Foster NL, Kuhl DE. Metabolic reduction in the posterior cingulate cortex in very early Alzheimer's disease. Ann Neurol 1997;42(1):85–94.
9. Alexopoulos P, Sorg C, Förschler A, et al. Perfusion abnormalities in mild cognitive impairment and mild dementia in Alzheimer's disease measured by pulsed arterial spin labeling MRI. Eur Arch Psychiatry Clin Neurosci 2012;262(1):69–77.
10. Williams DS, Detre JA, Leigh JS, Koretsky AP. Magnetic resonance imaging of perfusion using spin inversion of arterial water. Proc Natl Acad Sci U S A 1992;89(1):212–216.
11. Chen Y, Wolk DA, Reddin JS, et al. Voxel-level comparison of arterial spin-labeled perfusion MRI and FDG-PET in Alzheimer disease. Neurology 2011;77(22):1977–1985.
12. Musiek ES, Chen Y, Korczykowski M, et al. Direct comparison of fluorodeoxyglucose positron emission tomography and arterial spin labeling magnetic resonance imaging in Alzheimer's disease. Alzheimers Dement 2012;8(1):51–59.
13. Verfaillie SC, Adriaanse SM, Binnewijzend MA, et al. Cerebral perfusion and glucose metabolism in Alzheimer's disease and frontotemporal dementia: two sides of the same coin? Eur Radiol 2015;25(10):3050–3059.
14. Trebeschi S, Riederer I, Preibisch C, et al. Diagnostic Potential of Pulsed Arterial Spin Labeling in Alzheimer's Disease. Front Neurosci 2016;10:154.
15. McKhann G, Drachman D, Folstein M, Katzman R, Price D, Stadlan EM. Clinical diagnosis of Alzheimer's disease: report of the NINCDS-ADRDA Work Group under the auspices of Department of Health and Human Services Task Force on Alzheimer's Disease. Neurology 1984;34(7):939–944.
16. Winblad B, Palmer K, Kivipelto M, et al. Mild cognitive impairment—beyond controversies, towards a consensus: report of the International Working Group on Mild Cognitive Impairment. J Intern Med 2004;256(3):240–246.
17. Johnson NA, Jahng GH, Weiner MW, et al. Pattern of cerebral hypoperfusion in Alzheimer disease and mild cognitive impairment measured with arterial spin-labeling MR imaging: initial experience. Radiology 2005;234(3):851–859.
18. Herholz K. FDG PET and differential diagnosis of dementia. Alzheimer Dis Assoc Disord 1995;9(1):6–16.
19. Silverman DH, Small GW, Chang CY, et al. Positron emission tomography in evaluation of dementia: Regional brain metabolism and long-term outcome. JAMA 2001;286(17):2120–2127.
20. Jack CR Jr, Knopman DS, Jagust WJ, et al. Tracking pathophysiological processes in Alzheimer's disease: an updated hypothetical model of dynamic biomarkers. Lancet Neurol 2013;12(2):207–216.
21. Magistretti PJ. Neuron-glia metabolic coupling and plasticity. J Exp Biol 2006;209(Pt 12):2304–2311.
22. Attwell D, Buchan AM, Charpak S, Lauritzen M, Macvicar BA, Newman EA. Glial and neuronal control of brain blood flow. Nature 2010;468(7321):232–243.
23. Devor A, Sakadžić S, Srinivasan VJ, et al. Frontiers in optical imaging of cerebral blood flow and metabolism. J Cereb Blood Flow Metab 2012;32(7):1259–1276.
24. Stobart JL, Anderson CM. Multifunctional role of astrocytes as gatekeepers of neuronal energy supply. Front Cell Neurosci 2013;7:38.
25. Binnewijzend MA, Kuijer JP, Benedictus MR, et al. Cerebral blood flow measured with 3D pseudocontinuous arterial spin-labeling MR imaging in Alzheimer disease and mild cognitive impairment: a marker for disease severity. Radiology 2013;267(1):221–230.
26. Preibisch C, Sorg C, Förschler A, et al. Age-related cerebral perfusion changes in the parietal and temporal lobes measured by pulsed arterial spin labeling. J Magn Reson Imaging 2011;34(6):1295–1302.
27. Alsop DC, Detre JA, Golay X, et al. Recommended implementation of arterial spin-labeled perfusion MRI for clinical applications: A consensus of the ISMRM perfusion study group and the European consortium for ASL in dementia. Magn Reson Med 2015;73(1):102–116.
28. Grothe MJ, Teipel SJ; Alzheimer's Disease Neuroimaging Initiative. Spatial patterns of atrophy, hypometabolism, and amyloid deposition in Alzheimer's disease correspond to dissociable functional brain networks. Hum Brain Mapp 2016;37(1):35–53.
29. Guo X, Han Y, Chen K, Wang Y, Yao L. Mapping joint grey and white matter reductions in Alzheimer's disease using joint independent component analysis. Neurosci Lett 2012;531(2):136–141.
30. Liu K, Chen K, Yao L, Guo X. Prediction of Mild Cognitive Impairment Conversion Using a Combination of Independent Component Analysis and the Cox Model. Front Hum Neurosci 2017;11:33.
31. Ouyang X, Chen K, Yao L, et al. Simultaneous changes in gray matter volume and white matter fractional anisotropy in Alzheimer's disease revealed by multimodal CCA and joint ICA. Neuroscience 2015;301:553–562.
32. Shaffer JL, Petrella JR, Sheldon FC, et al. Predicting cognitive decline in subjects at risk for Alzheimer disease by using combined cerebrospinal fluid, MR imaging, and PET biomarkers. Radiology 2013;266(2):583–591.
33. Savio A, Fünger S, Tahmasian M, et al. Resting-State Networks as Simultaneously Measured with Functional MRI and PET. J Nucl Med 2017;58(8):1314–1317.
34. Toussaint PJ, Perlbarg V, Bellec P, et al. Resting state FDG-PET functional connectivity as an early biomarker of Alzheimer's disease using conjoint univariate and independent component analyses. Neuroimage 2012;63(2):936–946.
35. Chen J, Liu J, Calhoun VD, et al. Exploration of scanning effects in multi-site structural MRI studies. J Neurosci Methods 2014;230:37–50.
36. Xu L, Groth KM, Pearlson G, Schretlen DJ, Calhoun VD. Source-based morphometry: the use of independent component analysis to identify gray matter differences with application to schizophrenia. Hum Brain Mapp 2009;30(3):711–724.
37. Chen J, Calhoun VD, Arias-Vasquez A, et al. G-protein genomic association with normal variation in gray matter density. Hum Brain Mapp 2015;36(11):4272–4286.
38. Luo L, Xu L, Jung R, Pearlson G, Adali T, Calhoun VD. Constrained source-based morphometry identifies structural networks associated with default mode network. Brain Connect 2012;2(1):33–43.
39. Ciarochi JA, Calhoun VD, Lourens S, et al. Patterns of Co-Occurring Gray Matter Concentration Loss across the Huntington Disease Prodrome. Front Neurol 2016;7:147.
40. Ferreira LK, Diniz BS, Forlenza OV, Busatto GF, Zanetti MV. Neurostructural predictors of Alzheimer's disease: a meta-analysis of VBM studies. Neurobiol Aging 2011;32(10):1733–1741.